Inorganic Chemistry
Article

Inorg. Chem. **2009,** *48,* 4685–4691 **4685**
DOI:10.1021/ic900064m

Effects of Hydrothermal Temperature on the Microstructures of $BiVO_4$ and Its Photocatalytic O_2 Evolution Activity under Visible Light

Dingning Ke,[†] Tianyou Peng,*[,†,‡] Liang Ma,[†] Ping Cai,[†] and Ke Dai[†]

[†]*College of Chemistry and Molecular Science, Wuhan University, Wuhan 430072, China, and*
[‡]*State Key Laboratory Breeding Base of Photocatalysis, Fuzhou University, Fuzhou 350002, China*

Received September 9, 2008

Microspheric and lamellar $BiVO_4$ powders were selectively prepared through a hydrothermal process by using cetyltrimethylammonium bromide (CTAB) as a template-directing reagent. The as-prepared $BiVO_4$ powders were characterized by X-ray diffraction, electron microscopy, nitrogen adsorption−desorption experimentation, Fourier transform infrared spectrometry, and UV−vis diffuse reflectance spectroscopy. Experimental results indicate that microspheric $BiVO_4$ with particle sizes in the range of 7∼12 μm can be derived from a relatively low hydrothermal temperature (≤160 °C) and possess a mixed crystal consisting of tetragonal and monoclinic phases, whereas lamellar $BiVO_4$ with a pure monoclinic phase can be obtained at a higher hydrothermal temperature (200 °C). Their photocatalytic activities for O_2 evolution were investigated by using $Fe(NO_3)_3$ as a sacrificial reagent under visible-light irradiation, and the lamellar $BiVO_4$ shows a better photoactivity than the microspheric product due to its pure monoclinic crystal phase. Moreover, the effects of CTAB content on the morphologies and crystal phases of the obtained products were also discussed. It was found that the addition of CTAB can adjust the morphologies of $BiVO_4$ and obstruct the crystal phase transformation from the mixed crystal to pure monoclinic $BiVO_4$ during the hydrothermal process.

1. Introduction

Since photoelelctrochemical water-splitting into H_2 and O_2 on a TiO_2 electrode was reported in 1972,[1] various attempts of water photosplitting over semiconductors (e.g., TiO_2 and CdS) have been made with a view to constructing a solar energy conversion system for H_2 fuel production.[2−6] Among those, most investigations have focused on photocatalytic H_2 production on a photocatalyst, whereas O_2 evolution is much more difficult than the kinetically simpler process of H_2 evolution because it requires the abstraction of four electrons.[7,8] The inability to produce O_2 on a photocatalyst has prevented the construction of a water-splitting system for H_2 production.[8] Therefore, developing a novel photocatalyst for O_2 evolution is necessary for constructing an effective solar energy conversion system from water-splitting to H_2 fuel.[2,7,8]

It is well-known that WO_3 can photo-oxidize water into O_2 under visible-light irradiation,[9,10] but its band gap (ca. 2.8 eV) is still too large to efficiently absorb sunlight. Recently, bismuth vanadate ($BiVO_4$), generally used as a yellow pigment to replace cadmium-based material due to its low environmental toxicity, has inspired a great deal of research interest because of its excellent photoactivity under visible-light irradiation.[11−18] According to previous reports, $BiVO_4$ has three main crystal phases: a zircon structure with a tetragonal (z-t) system and a scheelite structure with a monoclinic (s-m) and a tetragonal (s-t) system.[19] Among

*To whom correspondence should be addressed. Tel.: +86-27-8721-8474. Fax: +86-27-6875-4067. E-mail: typeng@whu.edu.cn.

(1) Fujishima, A.; Honda, K. *Nature* **1972**, *238*, 37–38.
(2) Galińska, A.; Walendziewski, J. *Energy Fuels* **2005**, *19*, 1143–1147.
(3) Patsoura, A.; Kondarides, D.; Verykios, X. *Appl. Catal., A* **2006**, *64*, 171–179.
(4) Kitano, M.; Takeuchi, M.; Matsuoka, M.; Thomas, J.; Anpo, M. *Catal. Today* **2007**, *120*, 133–138.
(5) Sathish, M.; Viswanath, R. *Catal. Today* **2007**, *129*, 421–427.
(6) Jing, D.; Guo, L. *J. Phys. Chem. B* **2006**, *110*, 11139–11145.
(7) Sayama, K.; Mukasa, K.; Abe, R.; Abe, Y.; Arakawa, H. *Chem. Commun.* **2001**, 2416–2417.
(8) Sayama, K.; Mukasa, K.; Abe, R.; Abe, Y.; Arakawa, H. *J. Photochem. Photobiol., A* **2002**, *148*, 71–77.
(9) Bamwenda, G.; Arakawa, H. *Appl. Catal., A* **2001**, *210*, 181–191.
(10) Hameed, A.; Gondal, M.; Yamani, Z. *Catal. Commun.* **2004**, *5*, 715–719.
(11) Kohtani, S.; Koshiko, M.; Kudo, A. *Appl. Catal., B* **2003**, *46*, 573–586.
(12) Zhou, L.; Wang., W; Zhang, Z. L.; Xu, H. L.; Zhu, W. *J. Phys. Chem. C* **2007**, *111*, 13659–13664.
(13) Xie, B. P.; Zhang, H. X.; Cai, P. X.; Qiu, R.; Xiong, Y. *Chemosphere* **2006**, *63*, 956–963.
(14) Zhang, L.; Chen, D. R.; Jiao, X, L. *J. Phys. Chem. B* **2006**, *110*, 2668–2673.
(15) Kudo, A.; Omori, K.; Kato, H. *J. Am. Chem. Soc.* **1999**, *121*, 11459–11467.
(16) Kudo, A.; Ueda, K.; Kato, Hi.; Mikami, I. *Catal. Lett.* **1998**, *53*, 229–230.
(17) Yu, J. Q.; Kudo, A. *Adv. Funct. Mater.* **2006**, *16*, 2163–2170.
(18) Wood, P.; Glasser, F. P. *Ceram. Int.* **2004**, *30*, 875–882.
(19) Lim, A. R.; Choh, S. H.; Jang, M. S. *J. Phys.: Condens. Mater.* **1995**, *7*, 7309–7323.

Published on Web 4/28/2009

them, $BiVO_4$(s-m) is usually obtained through solid-state and melting reaction procedures, and $BiVO_4$(z-t) is prepared via precipitation processes from a $Bi(NO_3)_3$ and NH_4VO_3 solution at room temperature.[20] The phase transition between $BiVO_4$(s-m) and $BiVO_4$(s-t) is reversible at about 255 °C,[20] and $BiVO_4$(z-t) can be transformed into $BiVO_4$(s-m) after a heat treatment at 400∼600 °C.[19] Among the above three crystal phases, $BiVO_4$(s-m) is the best visible-light-driven photocatalyst for the degradation of organic pollutants and O_2 production from water-splitting due to its narrow band gap (ca. 2.4 eV),[11−14,21] while the photocatalytic activity of $BiVO_4$(z-t) is negligible.[15] For example, Kohtani and co-workers have found that $BiVO_4$(s-m) was able to photodegrade alkylphenols in wastewater under sunlight irradiation.[11] As a visible-light-driven photocatalyst, $BiVO_4$(s-m) has also been used to simultaneously photo-oxidize phenol and photoreduce Cr(VI).[13] Furthermore, excellent photocatalytic activities for O_2 evolution on $BiVO_4$(s-m) have also been observed under visible-light irradiation.[15−17]

$BiVO_4$ powders with various morphologies have been synthesized through different surfactant templating routes.[14,21,22] For example, nanofibroid $BiVO_4$(s-m) has been synthesized from cetyltrimethylammonium bromide (CTAB) solution in heptane and hexanol.[21] Flaky $BiVO_4$(s-m) has been hydrothermally synthesized in the presence of sodium dodecylbenzenesulfonate.[14] Recently, 3-D hierarchical nanostructures of $BiVO_4$ (s-m) have been synthesized through a simple hydrothermal process by using Gemini surfactant (C12-MADS) as a structure-directing reagent.[22] In this study, $BiVO_4$ powders with different morphologies were hydrothermally synthesized by using CTAB as a template-directing reagent. Microspheric and lamellar $BiVO_4$ particles were selectively prepared through adjustment of the hydrothermal temperature. The photocatalytic activities for O_2 evolution on the microspheric and lamellar $BiVO_4$ were comparatively investigated under visible-light irradiation. Moreover, the effects of hydrothermal temperature and surfactant content on the morphology and crystal phase of the obtained $BiVO_4$ were also discussed.

2. Experimental Section

2.1. Preparation of Materials. All chemicals used in the present experiments were obtained from commercial sources as analytical reagents. A typical synthesis process is as follows: 2.9100 g of $Bi(NO_3)_3 \cdot 5H_2O$ (Sinopharm Chemical Reagent Co. Ltd., 99%) and 0.7204 g of NH_4VO_3 (Sinopharm Chemical Reagent Co. Ltd., 99%) were dissolved into 30 mL of a 0.5 M HNO_3 solution under magnetic stirring in succession, and then 30 mL of a 0.03 M CTAB solution was added into the above mixture under vigorous stirring. The pH of the above mixture was adjusted to 6.00 with an ammonia solution. After aging for 12 h without stirring, the mixture was transferred into a Teflon-lined stainless steel autoclave and maintained at different temperatures for 72 h. The resultant solid was separated by centrifugation and washed with water and ethanol three times and then dried in the air. An anion-exchange treatment was performed by mixing the as-prepared sample (0.5000 g) with an ethanol solution of sodium acetate (40 mL, 0.05 M) under stirring at 40 °C for 72 h. The solid was washed with water and ethanol and then dried at 60 °C to obtain the product.

2.2. Characterization of Materials. X-ray diffraction (XRD) patterns were obtained with an XRD-6000 diffractometer using Cu Kα radiation (λ = 0.15418 nm). The morphologies were studied with a LaB_6 JEM-2010 (HT)-FEF transmission electron microscope (TEM) and an FEI Quanta 200 scanning electron microscope (SEM). The UV−vis diffuse reflectance absorption spectra were recorded on a Cary 5000 UV−vis−NIR spectrophotometer equipped with an integrating sphere using $BaSO_4$ as a reference. Fourier transform infrared (FTIR) spectra were acquired with a Thermo Nicolet Avatar 360 FTIR spectrometer. The Brunauer−Emmett−Teller (BET) surface areas of the samples were analyzed by nitrogen adsorption−desorption measurement using a Micromeritics ASAP 2020 apparatus after the samples were degassed at 180 °C.

2.3. Photocatalytic Activity Test. The photocatalytic O_2 evolution on a photocatalyst from an $Fe(NO_3)_3$ aqueous solution was carried out in a closed gas-circulation system. A 300 W Xe illuminator (CHF-XM-300W, Beijing Trusttech Co.) was used as a light source, which was collimated and focused into 5 cm^2 parallel faculae and then translated into upright light by a viewfinder. A cutoff filter (Kenko L-42) was employed for the visible-light irradiation (λ > 420 nm).

The photochemical reaction was performed in a reaction cell (Pyrex glass) containing the photocatalyst (0.100 g) and a 0.05 M $Fe(NO_3)_3$ solution (100 mL). Prior to the light irradiation, the above suspension was thoroughly degassed to remove air completely, and the reactor was irradiated from the top. The amount of evolved O_2 was determined with a gas chromatograph (GC, SP-6800A, thermal conductivity detector, 5 Å molecular sieve columns and Ar carrier).

Generally, quantum yield is an optimum parameter of the efficiency rating for a photochemical reaction system.[23,24] Chemical actinometry has also been tried to determine the quantum yield in the present system by employing potassium ferrioxalate according to previous literature accounts.[23] However, it was found that there exist some difficulties in making these measurements under the currently available conditions. Therefore, the time courses of photocatalytic O_2 evolution over the photocatalysts were applied in order to compare their photocatalytic efficiencies in the present work.

3. Results and Discussion

3.1. XRD Analyses of the $BiVO_4$ Powders. Figure 1 shows the XRD patterns of the products obtained at different hydrothermal temperatures. The products hydrothermally derived at 80, 120, and 160 °C reveal identical XRD patterns, as shown in Figure 1a−c, which can be ascribed to $BiVO_4$(z-t) (JCPD no: 14-0133) along with a few $BiVO_4$(s-m)'s (JCPD no: 14-0688).[25,26] The monoclinic $BiVO_4$ is slightly increased with a rise in the hydrothermal temperature from 80 to 160 °C. Once the hydrothermal temperature is reached (200 °C), pure $BiVO_4$(s-m) can be obtained, as observed in Figure 1d. This phenomenon is similar to the previous report that hydrothermal treatment at 200 °C is sufficient for the preparation of pure $BiVO_4$(s-m).[25] The formation of monoclinic $BiVO_4$ under a higher hydrothermal temperature strongly suggests that $BiVO_4$(s-m) is a thermodynamically stable phase, while $BiVO_4$(z-t) is a metastable one

(20) Tokunaga, S.; Kato, H.; Kudo, A. *Chem. Mater.* **2001**, *13*, 4624–4628.
(21) Yu, J.; Kudo, A. *Chem. Lett.* **2005**, *34*, 850–882.
(22) Zheng, Y.; Wu, J.; Duan, F.; Xie, Y. *Chem. Lett.* **2007**, *36*, 520–521.
(23) Sun, L.; Bolton, J. *J. Phys. Chem. B* **1996**, *100*, 4127–4134.
(24) Probst, B.; Kolano, C.; Hamm, P.; Alberto, R. *Inorg. Chem.* **2009**, *48*, 1836–1843.
(25) Zhang, X.; Ai, Z.; Jia, F.; Zhang, L.; Fan, X.; Zou, Z. *Mater. Chem. Phys.* **2007**, *103*, 162–167.
(26) Gotića, M.; Musića, S.; Ivandaa, M.; Šoufekb, M.; Popovic, S. *J. Mol. Struct.* **2005**, *744*, 535–540.

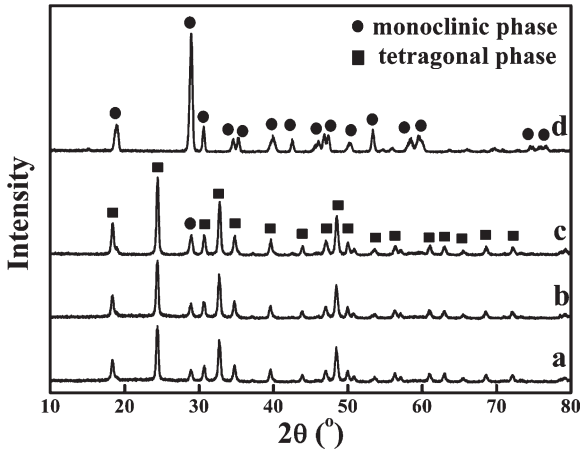

Figure 1. XRD patterns of $BiVO_4$ products derived from different hydrothermal temperatures for 72 h in the presence of 0.03 M CTAB. (a) 80 °C, (b) 120 °C, (c) 160 °C, and (d) 200 °C.

under the present experimental conditions.[27] However, further experimental results prove that a pure $BiVO_4$(s-m) can also be obtained at 160 °C by prolonging the hydrothermal time from 72 to 96 h (refer to the Supporting Information, Figure S1a). Therefore, it seems that the phase transformations of $BiVO_4$ are controlled both kinetically and thermodynamically, which should be further investigated.

3.2. Morphologies of the $BiVO_4$ Powders. The SEM and TEM images of $BiVO_4$ derived from different hydrothermal temperatures in the presence of 0.03 M CTAB are shown in Figures 2 and 3, respectively. As can be seen, the hydrothermal temperature has a significant influence on the morphology of the product. The panoramic view in Figure 2a clearly illustrates that $BiVO_4$ hydrothermally derived at 80 °C mostly consists of relative uniform microspheres with a diameter of 7∼12 μm, coexisting with many irregular nanoparticles. One individual microsphere with some attached irregular particles can be clearly observed from the inset in Figure 2a, which has a well-defined spherical shape with a diameter of ca. 10 μm. Figure 3a shows that the microspheres could possibly consist of aggregations containing nanoparticles and nanosheets with much smaller dimensions. The products derived at 120 and 160 °C also show similar morphologies; the slight difference is that there are much fewer irregular nanoparticles coexisting on the surfaces of microspheric particles in comparison with the product derived at 80 °C (Figure 2b and c). It is noticeable that some small cavities appeared on the surfaces of microspheres derived at 160 °C (Figure 2c), implying that the microspheres might be in a metastable state at this elevated temperature. Figure 2d shows that the product hydrothermally derived at 200 °C is a well-defined lamellar structure with dimensions in the range of 0.08∼0.12 μm. Those lamellae are composed of terracelike particles with no spherical particles, and those terraces are stepped along the edges of lamellae (Figures 2d and 3b). The above observations imply that those terracelike lamellae might be transformed from the nanoparticles and nanosheets, as shown in Figure 3a. These

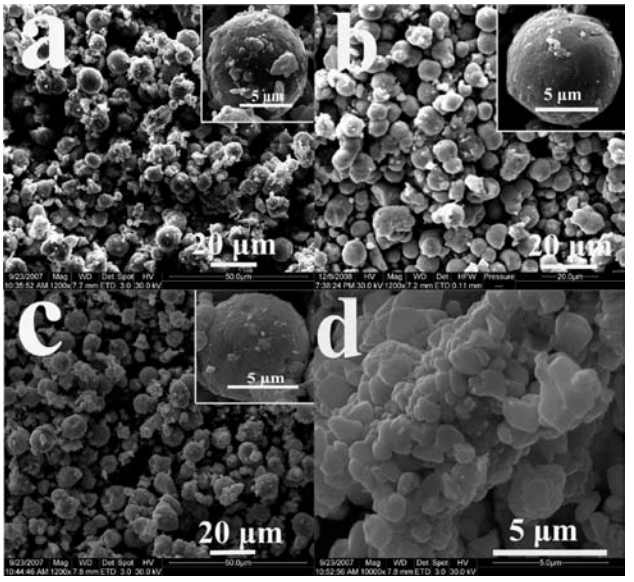

Figure 2. Typical SEM images of $BiVO_4$ products obtained at different hydrothermal temperatures for 72 h in the presence of 0.03 M CTAB. (a) 80 °C, (b) 120 °C, (c) 160 °C, and (d) 200 °C.

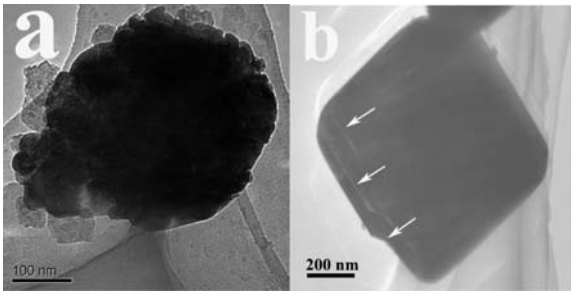

Figure 3. Typical TEM images of $BiVO_4$ products obtained at different hydrothermal temperatures for 72 h in the presence of 0.03 M CTAB. (a) 80 °C and (b) 200 °C.

nanoparticles and nanosheets in the microspheric aggregations (Figures 2a−c and 3a) can grow and accumulate to form those terracelike lamellae along with the phase transformation from a mixed crystal to $BiVO_4$(s-m) (Figure 1) under hydrothermal treatment at 200 °C. Although it has been reported that $BiVO_4$ with various morphologies could be synthesized by different surfactant templating routes,[14,21,22] the present $BiVO_4$ with microspheric and lamellar morphologies in the presence of CTAB has not been reported before. The relevant formation mechanism and the role of the surfactant will be further discussed in detail in the following section.

3.3. UV−Vis Diffuse Reflectance Absorption Spectra of $BiVO_4$ Powders. Figure 4 displays the diffuse reflectance absorption spectra of $BiVO_4$ prepared at different hydrothermal temperatures in the presence of 0.03 M CTAB. All of the products show excellent visible-light absorption, and the product hydrothermally produced at 200 °C shows the best visible-light response. Its absorption edge is estimated to be 549 nm with a band gap of 2.26 eV, which can be ascribed to the characteristic absorption of $BiVO_4$(s-m).[15] However, the absorption edge (537 nm) of $BiVO_4$ derived at 80 °C is similar to those of products prepared at 120 and 160 °C, and their corresponding band gaps are calculated to be 2.31, 2.30,

(27) Stoltzfus, M. W.; Woodward, P. M.; Seshadri, R.; Klepeis, J. H.; Bursten, B. *Inorg. Chem.* **2007**, *46*, 3839–3850.

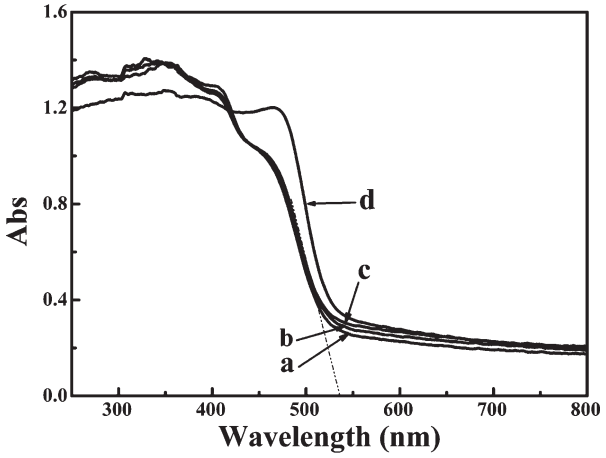

Figure 4. UV−vis diffuse reflectance absorption spectra of $BiVO_4$ products derived from different hydrothermal temperatures for 72 h in the presence of 0.03 M CTAB. (a) 80 °C, (b) 120 °C, (c) 160 °C, and (d) 200 °C.

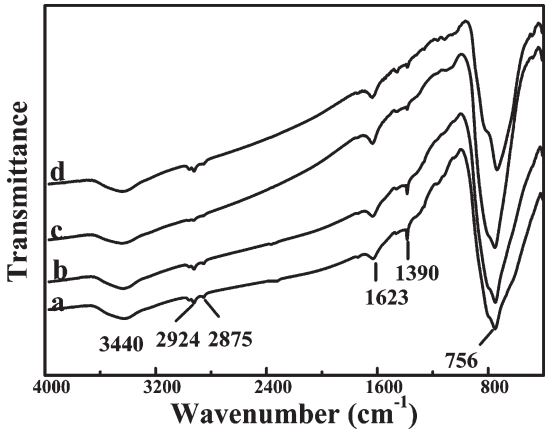

Figure 5. FTIR spectra of $BiVO_4$ products derived from different hydrothermal temperatures for 72 h in the presence of 0.03 M CTAB. (a) 80 °C, (b) 120 °C, (c) 160 °C, and (d) 200 °C.

and 2.29 eV, respectively. Clearly, the absorption edge slightly shifts to red light with an elevation of the hydrothermal temperature from 80 to 200 °C.

As demonstrated before, the visible-light absorption band with an absorption edge of 430 nm for $BiVO_4$(z-t) is assigned to the electron transition from an O_{2p} valence band to a V_{3d} conduction band,[15] while the valence bands at the top of the $BiVO_4$(s-m) may be formed by both O_{2p} (64%) and Bi_{6s} (18%), namely, a hybrid orbital of Bi_{6s} and O_{2p} ($Bi_{6s}-O_{2p}$). [28] The presence of Bi_{6s} in the top of the valence bands results in a more negative energy level of the valence band and then a decrease in the band gap.[28] The absorption edges of the present products obtained at 80, 120, and 160 °C show an obvious red shift in comparison to a pure $BiVO_4$(z-t) with an absorption edge of 430 nm.[15] According to the XRD analytical results, the above products are mixtures containing mostly a tetragonal phase and a few monoclinic phases. Therefore, it is reasonable to conclude that the coexisting $BiVO_4$(s-m) contributed to the above red shifts in the absorption band for the present products. This phenomenon of the top of the valence band being controlled by the Bi_{6s} or hybrid $Bi_{6s}-O_{2p}$ orbital is expected to provide valuable information for the development of novel visible-light-driven photocatalysts.

3.4. Infrared Spectra of the $BiVO_4$ powders. Figure 5 shows the FTIR spectra of the $BiVO_4$ derived from different hydrothermal temperatures. The obvious absorptions at 1623 cm^{-1} and 3440 cm^{-1} can be ascribed to bending and stretching vibrations of the adsorbed H_2O molecules, respectively.[29] The medium peak at 1390 cm^{-1} and the weak peak at 1440 cm^{-1} indicate adsorbed trace NO_3^-.[29,30] The very weak absorption bands at 2924, 2875, and 1052 cm^{-1} can be ascribed to aliphatic C−H and C−N stretching vibrations,[31] respectively. It suggests that CTAB can be efficiently removed by the ion-exchange and washing processes due to the relative weak bonding between CTAB and $BiVO_4$.[32]

The $BiVO_4$ hydrothermally derived at 80 °C is characterized by a very strong absorption band at 756 cm^{-1} with a shoulder at 818 cm^{-1} (V−O),[26] which is similar to that of $BiVO_4$ obtained at 120 and 160 °C. However, the strong absorption band and a weak shoulder absorption band of V−O for the product prepared at 200 °C show a blue shift (731 cm^{-1}) and a red shift (827 cm^{-1}), respectively. This may be attributable to the crystal phase transformation from $BiVO_4$ (z-t) to $BiVO_4$ (s-m). In this process, the unit cell volume of $BiVO_4$ reduced from 351.2 $Å^3$ for $BiVO_4$(z-t) to 309.2 $Å^3$ for $BiVO_4$(s-m).[27] The VO_4 tetrahedron in $BiVO_4$(z-t) has four equivalent distances (4×1.74 Å), whereas the V^{5+} ion in the monoclinic phase was located in a distorted tetrahedral environment with two different V−O distances (2×1.68 Å, 2×1.77 Å).[25] Those differences in the two crystal phases would induce absorption band shifts, as shown in the FTIR spectra, which should be further ascertained.

3.5. Photocatalytic Properties of the $BiVO_4$ Powders. Figure 6 shows the time courses of photocatalytic O_2 evolution from various $BiVO_4$ suspension systems containing an $Fe(NO_3)_3$ aqueous solution under visible-light ($\lambda > 420$ nm) irradiation. $BiVO_4$(s-m) derived at 200 °C exhibits the best O_2 evolution efficiency (549 μmol h^{-1}) at the first 1 h of irradiation among all of the products tested, which can be attributed to its pure monoclinic phase and a most excellent visible-light response (Figures 1d and 4d). This is consistent with the previous report that $BiVO_4$(s-m) possesses higher photocatalytic activity than $BiVO_4$(z-t) under visible light.[15,25] The products hydrothermally derived at 80∼160 °C also show obvious photocatalytic O_2 evolution efficiency, although they are mainly composed of $BiVO_4$(z-t) coexisting with limited $BiVO_4$(s-m). Figure 6 also reveals that photocatalytic O_2 evolution efficiency over the products is pronounced with the increase of the hydrothermal temperature from 80 to 160 °C, although they possess similar mixed crystals, light absorptions, and morphologies. The volume percentage of $BiVO_4$(s-m) in the products increases with an elevation of the hydrothermal tempera-

(28) Oshikiri, M.; Boero, M.; Ye, J.; Zou, Z.; Kido, G. *J. Chem. Phys.* **2002**, *117*, 7313–7318.
(29) García, J.; López, T.; Álvarez, M.; Aguilar, H.; Quintana, P. *J. Non-Cryst. Solids* **2008**, *354*, 729–732.
(30) Kanagadurai, R.; Sankar, R.; Sivanesan, G.; Srinivasan, S.; Rajasekaran, R.; Jayavel, R. *Mater. Chem. Phys.* **2008**, *108*, 170–175.
(31) Manjula, P.; Manonmani, S.; Fayaram, P.; Rajendran, S. *Anti-Corros. Methods Mater* **2001**, *48*, 319–323.
(32) Yada, M.; Mihara, M.; Mori, S.; Kuroki, M.; Kijima, T. *Adv. Mater.* **2002**, *14*, 309–313.

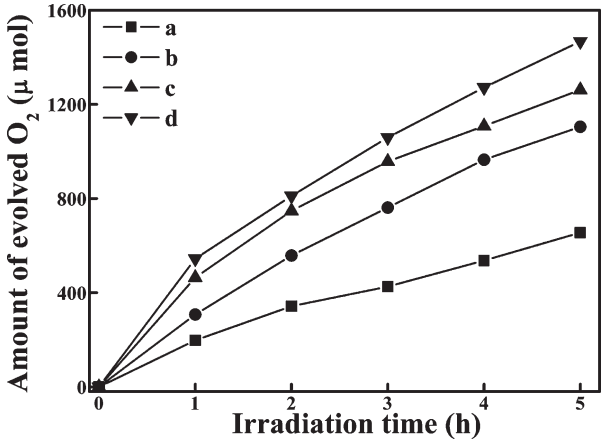

Figure 6. Time courses of photocatalytic O_2 evolution over various $BiVO_4$ products in the presence of $Fe(NO_3)_3$ solution under visible-light irradiation ($\lambda > 420$ nm). (a) 80 °C, (b) 120 °C, (c) 160 °C, and (d) 200 °C.

Table 1. BET Surface Areas and $BiVO_4$(s-m) Percentages in the Products Prepared at Different Hydrothermal Temperatures

hydrothermal temp. (°C)	80	120	160	200
S_{BET} ($m^2\ g^{-1}$)	2.04	1.59	1.04	0.32
$BiVO_4$(s-m) percentage[a] (%)	19.07	21.51	23.75	~100

[a] Calculated according to $V_{Monoclinic} = I_{Monoclinic(121)}/(I_{Monoclinic(121)} + I_{Tetragonal(200)})$ from XRD patterns.

ture from 80 to 160 °C, as shown in Table 1, and an increasing volume percentage of $BiVO_4$(s-m) usually leads to the delocalization and mobility of photogenerated carriers due to its relative low symmetry of $BiVO_4$-(s-m).[27] This improved mobility of the charge carriers can efficiently retard the recombination and then improve its photoactivity.[17]

It is well-known that a high specific surface area is usually beneficial for the adsorption of reactants, which might increase a reaction's chances between the photogenerated carriers and the reactants and then lead to a better photoactivity.[33] As observed in Table 1, although all of the products obtained show relatively small BET surface areas (S_{BET}), the S_{BET} value decreases upon enhancing the hydrothermal temperature from 80 to 200 °C, and the pure $BiVO_4$(s-m) derived at 200 °C possesses the smallest one. The products derived from a relatively low temperature (e.g., ≤ 160 °C) exhibit an increase in photocatalytic activity along with a decrease in the S_{BET} value, and the pure $BiVO_4$(s-m) possesses the best photoactivity, though the smallest surface area. It seems that the crystal phase is the decisive factor in the photoactivity, in comparison with the specific surface area in under present conditions.

On the basis of the above discussions and our previous results,[34] a conclusion might be drawn that the photogenerated holes in the valence band can oxidize the water to form O_2 while the photogenerated electrons in the conduction band can reduce Fe^{3+} to form Fe^{2+} under the present experimental conditions, because it is necessary that Fe^{3+} effectively captures the photogenerated electrons to avoid the carrier's recombination in the continuous O_2 production process. Therefore, the overall O_2 evolution reaction under the present conditions could be approximately suggested as follows:

$$4OH^- + 4Fe^{3+} \xrightarrow[BiVO_4]{h\nu>420\ nm} 2H_2O + O_2 + 4Fe^{2+} \quad \Delta H = 186\ kJ\ mol^{-1}$$

3.6. Discussion on the Formation Mechanism of Microspheric or Lamellar $BiVO_4$. As described above, $BiVO_4$(z-t) and $BiVO_4$(s-m) coexist in the products derived at relatively low hydrothermal temperatures (e.g., ≤ 160 °C). Moreover, the precipitate during the preparation of the hydrothermal mixture also showed a similar mixed crystal (refer to the Supporting Information, Figure SI1b). Those phenomena seem to suggest that the hydrothermal temperature was not an exclusive factor for the selective preparation of the crystal phase of $BiVO_4$. For example, highly crystalline $BiVO_4$(z-t) and $BiVO_4$(s-m) were selectively synthesized by changing the ratio of layered potassium vanadate to $Bi(NO_3)_3$ in aqueous media at room temperature.[15] An insufficient amount of vanadate in the reactant led to the formation of $BiVO_4$(z-t), whereas an excessive amount of vanadate led to the formation of $BiVO_4$(s-m).[15]

In the present preparation process of the hydrothermal mixture, vanadium species were first precipitated as reddish-brown V_2O_5 and then partly dissolved as VO_3^- under the present high acidity (pH = 0.80).[35] After adjusting the mixture to a pH of 6.0, it is considered part of the formation process that the above insufficient amounts of VO_3^- and BiO^+ slightly dissolved in water to form a $BiVO_4$ crystal nucleus due to electrostatic force. Those nuclei would congregate and grow to become a metastable precipitate. The main composition of $BiVO_4$(z-t) in the products without hydrothermal treatment might be attributable to the insufficient amount of VO_3^-, as described above. During the hydrothermal treatment at relatively low temperatures (e.g., 80~160 °C), those metastable $BiVO_4$ precipitates would reconstruct to form microspheric particles containing a mixed crystal of $BiVO_4$(z-t) and $BiVO_4$(s-m) under the surfactant-directing interaction and the hydrothermal conditions. Once the temperature was enhanced to 200 °C, pure $BiVO_4$(s-m) completely formed due to the thermodynamic factor.

Control experiments indicated that the microspheric and lamellar $BiVO_4$ could not be formed without the addition of CTAB; thus, the effect of CTAB on the morphologies of the products was further investigated. Figure 7 shows the SEM images of products derived from different CTAB concentrations and hydrothermal temperatures. As can be seen, irregular aggregations (Figure 7a) were derived from hydrothermal treatment at 80 °C for 72 h in the presence of 0.01 M CTAB. With enhancement of the CTAB concentration to 0.02 M, some microspheres with irregular shape began to appear and were covered with fibroid nanoparticles, as observed in

(33) Bao, N.; Shen, L.; Takata, T.; Domen, K. *Chem. Mater.* **2008**, *20*, 110–117.
(34) Ke, D.; Peng, T.; Ma, L.; Cai, P.; Jiang, P. *Appl. Catal., A* **2008**, *350*, 111–117.
(35) Chen, L.; Liu, Y.; Lu, Z.; Zeng, D. *J. Colloid Interface Sci.* **2006**, *295*, 440–444.

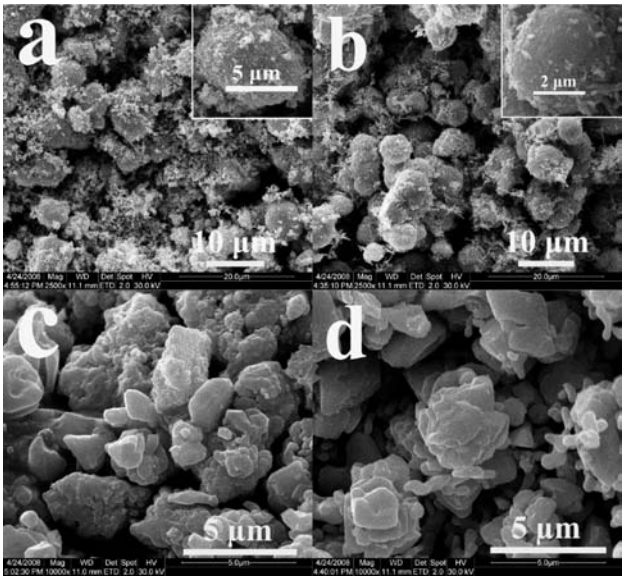

Figure 7. SEM images of products synthesized from different hydrothermal conditions. (a), (c) 0.01 M CTAB; (b), (d) 0.02 M CTAB; (a), (b) 80 °C hydrothermal treatment for 72 h; (c), (d) 200 °C hydrothermal treatment for 72 h.

Figure 7b, and then much more regular microspheres could be obtained from a mixture containing 0.03 M CTAB (Figure 2a). However, once the hydrothermal temperature was enhanced to 200 °C, irregular aggregations and a bit of lamellae were observed from the product prepared in the presence of 0.01 M CTAB (Figure 7c), and the lamellar structures became more uniform (Figures 7d and 2d) with a further increase in the CTAB concentration to 0.02 and 0.03 M CTAB. However, further experimental results demonstrated that much more irregular particles were formed in the absence of CTAB at the same hydrothermal temperature (refer to the Supporting Information, Figures SI 2a and 2d). Therefore, it is reasonable to conclude that the formation of microspheric or lamellar morphology was attributed to not only the presence of CTAB but also the hydrothermal temperature in the present system.

To further study the effect of CTAB on the crystal phase of $BiVO_4$, a set of $BiVO_4$ products was prepared under the same hydrothermal conditions in the absence of CTAB. As can be seen in Figure 8, the crystal phases of products obtained at 80 and 120 °C were an admixture containing dominant $BiVO_4$(z-t) with limited $BiVO_4$(s-m), which is similar to the product prepared in the presence of 0.03 M CTAB at the same temperature. The differences between them are that the proportion of the monoclinic phase obtained in the absence of CTAB is slightly higher than those gained in the presence of CTAB. Once the hydrothermal temperature rose to 160 °C, pure $BiVO_4$(s-m) could be obtained and lamellae-like particles appeared (refer to the Supporting Information, Figure SI 2c), suggesting that this temperature is sufficient for the preparation of pure $BiVO_4$(s-m) without CTAB. However, pure $BiVO_4$(s-m) was not obtained in the presence of CTAB until the hydrothermal temperature was enhanced to 200 °C. Therefore, the addition of CTAB might obstruct the crystal phase transformation from the mixed crystal to pure $BiVO_4$(s-m) at 160 °C.

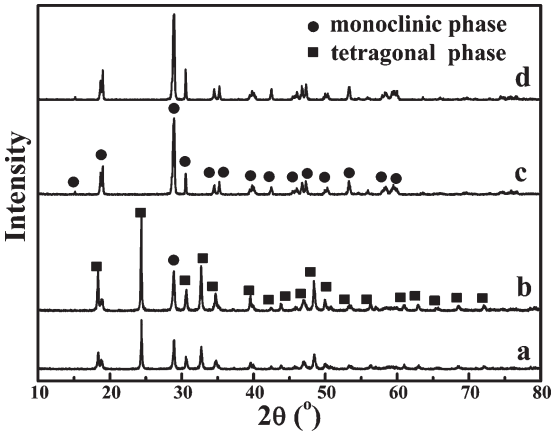

Figure 8. XRD patterns of $BiVO_4$ products derived from different hydrothermal temperatures for 72 h in the absence of CTAB. (a) 80 °C, (b) 120 °C, (c) 160 °C, and (d) 200 °C.

On the basis of the above-mentioned observations, the formation mechanisms of the different crystal phases and morphologies of $BiVO_4$ were proposed in Figure 9. Under the present experimental conditions, the VO_3^- and BiO^+ slightly dissolved in water to yield a $BiVO_4$ crystal nucleus due to electrostatic force, and then yielded a metastable precipitate. Under the surfactant-mediated interaction and hydrothermal conditions, those metastable precipitates reconstructed and grew into a $BiVO_4$ precipitate along with bilayer CTAB absorbed on the surfaces of produced $BiVO_4$.[36−38]

The energies of structures exhibiting distorted Bi^{3+} environments (e.g., monoclinic $BiVO_4$) are competitive with those possessing symmetric Bi^{3+} environments (e.g., tetragonal $BiVO_4$).[27] The relative contraction of the filled Bi_{6s} orbital can interact with the O_{2p} orbital, resulting in a mild destabilization of the symmetric structures (e.g., tetragonal $BiVO_4$). For the Bi^{3+} at low symmetry (e.g., monoclinic $BiVO_4$), antibonding $Bi_{6s}-O_{2p}$ states can mix with the unfilled Bi_{6p} orbital to produce a localized, nonbonding state at the top of the valence band, which leads to a reduction of the above destabilizing effect.[27] It is consistent with the present experiment results that $BiVO_4$(s-m) is the thermodynamically stable form and $BiVO_4$(z-t) is a metastable one. Moreover, it also suggests that a higher symmetric environment in $BiVO_4$(z-t) facilitates the adsorption of CTAB symmetrically, which leads to the formation of microspheric particles, as shown in Figure 2a−c.

At a higher hydrothermal temperature (e.g., 200 °C), the atom density on the (010) crystal plane of $BiVO_4$(s-m) is larger than those on the other planes,[14] which might provide an opportunity for adsorption of the ammonium radicals and then induce the formation of lamellar structures along with the phase transformation from tetragonal to monoclinic $BiVO_4$. Moreover, the higher internal pressure can be thought of as another impetus for the transformation from microspheric to lamellar $BiVO_4$, because it could destroy the adsorbed CTAB bilayers

(36) Sifaoui, H.; Ługowska, K.; Dománska, U.; Modaressi, A.; Rogalski, M. *J. Colloid Interface Sci.* **2007**, *314*, 643–650.
(37) Ducker, A.; Wanless, J. *Langmuir* **1999**, *15*, 160–168.
(38) Vakarelski, I.; Toritani, A.; Nakayama, M.; Higashitani, K. *Langmuir* **2003**, *19*, 110–117.

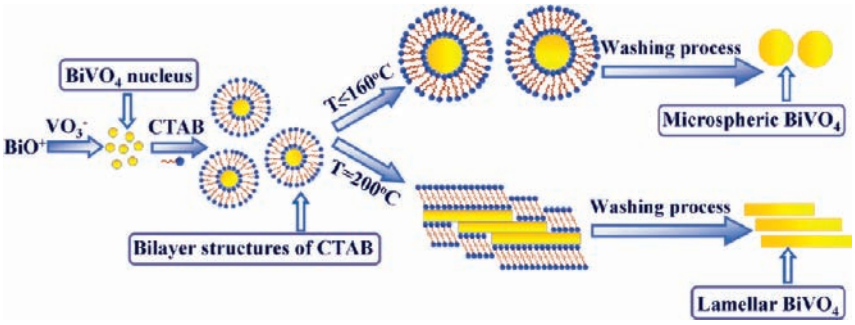

Figure 9. Schematic model of the formation mechanism for the microspheric and lamellar $BiVO_4$ products derived from different hydrothermal conditions.

and microspheric particles and then bring those partly unwarped particles and fragments together, which is also beneficial for the morphology transformation.[38]

4. Conclusions

Microspheric and lamellar $BiVO_4$ were prepared selectively by adjusting the hydrothermal temperature in the presence of CTAB, and its photocatalytic activity was investigated. It was found that the hydrothermal temperature significantly influenced the morphology, crystal phase, light absorption, and photocatalytic activity of the obtained $BiVO_4$. The microsphere $BiVO_4$ can be derived from a relatively low hydrothermal temperature (e.g., $\leq$ 160 °C) and possesses a mixed crystal consisting of tetragonal and monoclinic phases, whereas the lamellar $BiVO_4$ with a pure monoclinic phase can be obtained at a higher hydrothermal temperature (200 °C), which showed the best photocatalytic activity for O_2 evolution compared with the microspheric products with a mixed crystal of tetragonal and monoclinic phases. The lamellar $BiVO_4$ exhibited promising application as a visible-light-driven photocatalyst for photocatalytic O_2 production. Moreover, experimental results demonstrated that CTAB acted as a morphology-directing reagent for the formation of microspheric and lamellar $BiVO_4$, and CTAB might obstruct the crystal phase transformation from a mixed crystal to pure monoclinic $BiVO_4$ at 160 °C. The peculiar formation mechanism of microspheric and lamellar $BiVO_4$ is revealed here for the first time, which would be helpful for providing a deeper understanding of crystal growth during the hydrothermal process.

Acknowledgment. This work was supported by the National High-Tech Research and Development Program (2006AA03Z344), Program for New Century Excellent Talents in University (NCET-07-0637), and Natural Science Foundation of China (20573078).

Supporting Information Available: XRD patterns and SEM images of of $BiVO_4$. This material is available free of charge via the Internet at http://pubs.acs.org.